ACSNANO

www.acsnano.org

ARTICLE

Visualizing Heterogeneity of Monodisperse CdSe Nanocrystals by Their Assembly into Three-Dimensional Supercrystals

Elena V. Shevchenko,* Paul Podsiadlo, Xiaohua Wu, Byeongdu Lee, Tijana Rajh, Rachel Morin, and Matthew Pelton*

Cite This: https://dx.doi.org/10.1021/acsnano.0c04864

Read Online

ACCESS | Metrics & More | Article Recommendations | Supporting Information

ABSTRACT: We show that the self-assembly of monodisperse CdSe nanocrystals synthesized at lower temperature (~310 °C) into three-dimensional supercrystals results in the formation of separate regions within the supercrystals that display photoluminescence at two distinctly different wavelengths. Specifically, the central portions of the supercrystals display photoluminescence and absorption in the orange region of the spectrum, around 585 nm, compared to the 575 nm photoluminescence maximum for the nanocrystals dispersed in toluene. Distinct domains on the surfaces and edges of the supercrystals, by contrast, display photoluminescence and absorption in the green region of the spectrum, around 570 nm. We attribute the different-colored domains to two subpopulations of NCs in the monodisperse ensemble: the nanocrystals in the "orange" regions are chemically stable, whereas the nanocrystals in the "green" regions are partially oxidized. The susceptibility of the "green" nanocrystals to oxidation indicates a lower coverage of capping molecules on these nanocrystals. We propose that the two subpopulations correspond to nanocrystals with different surfaces that we attribute to the polytypism of CdSe.

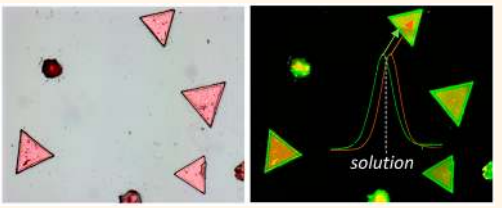

KEYWORDS: *self-assembly, nanocrystals, superlattices, photoluminescence, polytypism, polymorphism*

The synthesis of monodisperse spherical CdSe nanocrystals (NCs)[1] led shortly afterward to their use as building blocks for more complex, hierarchical structures, such as ordered three-dimensional (3D) assemblies.[2] CdSe NCs with different shapes such as nanorods, tetrapods, or even atomically flat nanoplates have been synthesized in solution and organized from the solution into 3D assemblies,[3−8] driven by interactions among neighboring particles.[9]

Periodic NC structures can be obtained by evaporation of the solvent[10−14] or by the destabilization of the colloidal solution by nonsolvent.[15−18] Solvent evaporation typically enables the fabrication of continuous long-range periodic films, whereas solution destabilization[15,19] results in the growth of 3D supercrystals (SCs) with symmetries similar to those of atomic inorganic crystals.[17,20] Monodisperse NCs can form face-centered cubic,[17] body-centered cubic,[17] simple hexagonal,[21] face-centered tetragonal, and other lattices. Multicomponent mixtures enable the creation of an extended library of periodic structures isostructural with atomic lattices.[11,12,22,23] In multicomponent mixtures, NCs can have the same or different surface chemistries, sizes, and compositions.

Here, we report an unusual effect in individual 3D SCs assembled by the destabilization of a solution of monodisperse CdSe NCs synthesized at ~310 °C. The majority of each SC emits light that is red-shifted compared to the corresponding NC solution, whereas some outer regions of the SCs emit blue-shifted light. For the nanocrystal sizes we used, these correspond to red-emitting and green-emitting regions. SCs assembled from CdSe NCs synthesized at higher temperature (380 °C) do not show bimodal light emission. We attribute the bimodal light emission to two subpopulations of NCs in the ensemble of NCs, with one population having lower ligand coverage than the other. The NCs with lower ligand coverage precipitate later than the NCs with higher ligand coverage and thus form the outer regions of the SCs. The lower ligand coverage also makes these NCs subject to oxidation, shifting their luminescence and absorption to shorter wavelengths. We hypothesize that the NCs with lower coverage correspond to those with a zinc blende (ZB) crystal structure on their

Received: June 10, 2020
Accepted: October 12, 2020

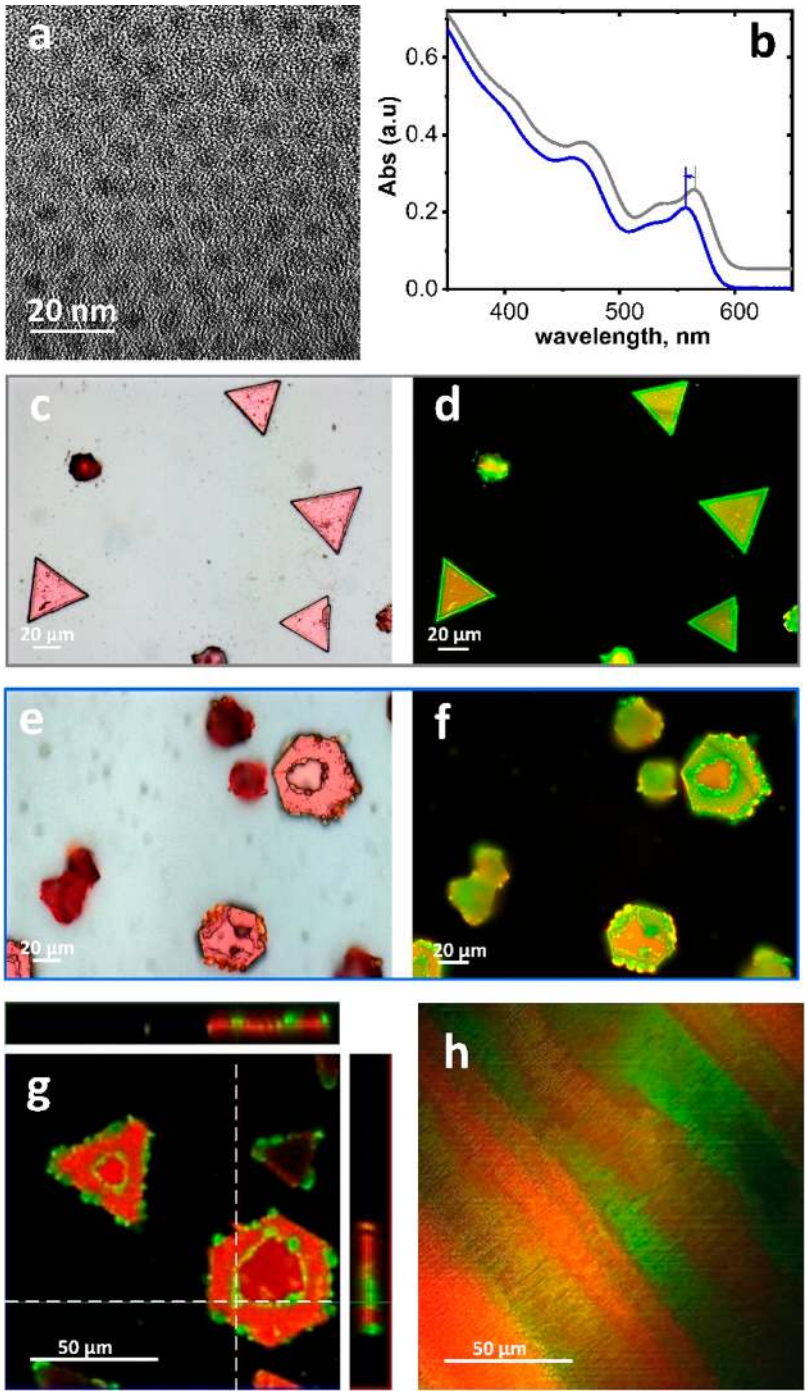

Figure 1. (a) Transmission electron micrograph of 4.6 nm CdSe nanocrystals. (b) Absorption spectra of dilute solutions of 4.4 nm (gray curve) and 4.6 nm (blue curve) CdSe nanocrystals in toluene. (c–f) Representative reflected-light optical micrographs (c,e) and corresponding fluorescence micrographs (d,f) of several three-dimensional supercrystals formed from 4.4 nm (c,d) and 4.6 nm (e,f) CdSe nanocrystals by controlled destabilization of the solution. (g) Laser scanning confocal micrograph of supercrystals; side images are cross sections (*z*-stacks) along the indicated (white dashed) lines. The stacks are 20 μm in depth. (h) Laser scanning confocal micrograph of a dried film of the nanocrystals.

surfaces, whereas those with higher ligand coverage have wurtzite (W) crystal structure on their surfaces.

RESULTS AND DISCUSSION

Figures 1a and S1 show transmission electron microscopy (TEM) images of monodisperse 4.4 and 4.6 nm CdSe NCs stabilized with trioctylphosphine oxide (TOPO), trioctylphosphine (TOP), and hexadecylamine (HDA),[17,19] and Figure 1b shows the corresponding narrow absorption spectra (half-width at half-maximum of the first excitonic peak = 35 nm). The optical spectra are indicative of a monodisperse ensemble of nanocrystals; this is confirmed by analysis of TEM images (Figure S2), which shows a Gaussian size distribution for each sample of CdSe NCs, with no indication of a bimodal distribution. Gentle destabilization of colloidal solutions of these NCs resulted in the formation of SCs of various shapes,

https://dx.doi.org/10.1021/acsnano.0c04864
ACS Nano XXXX, XXX, XXX–XXX

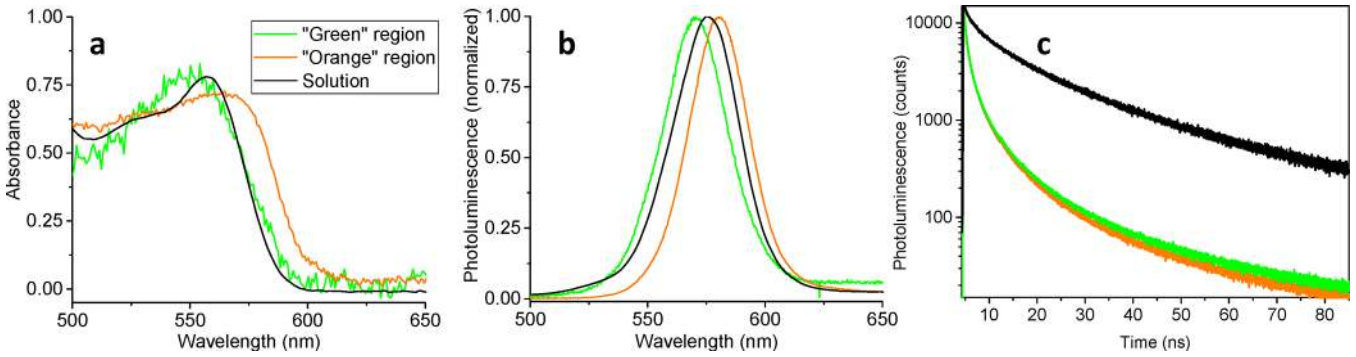

Figure 2. Characteristic spatially resolved (a) absorbance spectra, (b) photoluminescence spectra, and (c) time-resolved photoluminescence decay curves for blue-shifted ("green") and red-shifted ("orange") regions within individual SCs formed from 4.4 nm CdSe nanocrystals. The microscopic measurements have a spatial resolution of approximately 200 nm. Also shown for comparison are results for nanocrystals dispersed in toluene solution.

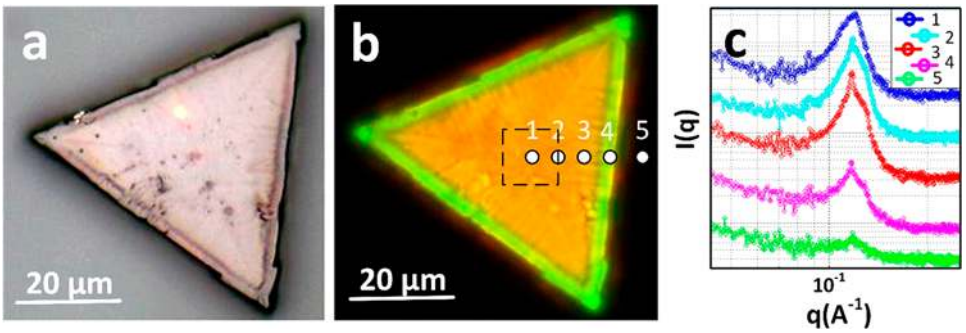

Figure 3. (a,b) Reflected light optical micrograph (a) and corresponding fluorescence image (b) of a supercrystal assembled from 4.6 nm CdSe nanocrystals. (c) Small-angle X-ray scattering spectra measured from five selected spots on the nanocrystal, as indicated in (b). The square represents the approximate size of the X-ray spot.

with lateral dimensions up to 80 μm (Figure 1c,e).[16,17] Scanning electron microscopy (SEM) images of SCs are shown in Figure S3. Such SCs were previously reported to have a face-centered cubic lattice structure.[2,16,17]

Fluorescence images of individual SCs revealed a coexistence of green-emitting and orange-emitting regions (Figure 1d,f). We made repeated measurements on the same samples over several months, and the green- and red-emitting regions were observed to be stable over this entire time. The green regions form distinct domains that are located primarily along the edges of the SCs. The formation of distinct green- and orange-emitting regions occurs for a wide variety of SCs, regardless of their overall shape or morphology (Figure S4).

Comparison of the reflected light and fluorescence images clearly shows the integrity of the different regions. 3D composite images obtained from laser scanning confocal microscopy (Figures 1g and S5) show that the different regions penetrate through the interior of the SCs and all the way to the substrate. The green regions appear less ordered in the fluorescence and confocal images, having irregular shapes and boundaries compared to the faceted appearance of the orange regions. In addition, randomly packed films of the same 4.4 nm NCs also exhibited orange- and green-emitting regions (Figure 1h). We note that the NCs were washed before deposition of the disordered films so that the number of ligands in the films is similar to the number of ligands in the SCs, as confirmed by thermogravimetric analysis (Figure S6).

To obtain more information about the optical properties of the "green" and "orange" regions, we made spatially resolved measurements of the photoluminescence (PL) and absorption spectra of the SCs. Compared to solutions of the same NCs, the "orange" regions of the SC exhibit both absorption and PL at lower energies, and the "green" regions exhibit both absorption and PL at higher energies (Figure 2a,b).

The red shift of the PL in the orange regions could potentially be attributed to energy transfer among the NCs in the SCs[2,24−28] or to luminescence from near-band-edge defect states.[29] However, these phenomena would not explain the red shift of the absorption in the same regions and are inconsistent with the symmetric PL spectra observed from all spots. Instead, we attribute the red shift to the local field effect, that is, to the higher dielectric constant of the NC environment in the SC compared to the dielectric constant in solution.[30]

In the green-emitting regions, this dielectric-induced red shift is compensated by an opposing blue shift, resulting in absorption at wavelengths slightly lower than those for NCs in solution. Although the different PL wavelengths in the two regions could be attributable to energy transfer, charge transfer, or trapping, none of these explanations can account for the bimodal nature of absorption wavelengths in the two regions. As further evidence that these processes are not responsible for the observed spectral shifts, we note that the PL dynamics in the orange and green regions are nearly identical to one another. We therefore conclude that the spectral shifts arise because NCs in the green regions have a higher effective band gap (*i.e.*, higher confinement energy) than NCs in the orange regions.

As the green regions tend to be located at the surfaces of the SCs, it could be hypothesized that the different colors are due to segregation of smaller NCs from larger NCs in solution,

https://dx.doi.org/10.1021/acsnano.0c04864
ACS Nano XXXX, XXX, XXX−XXX

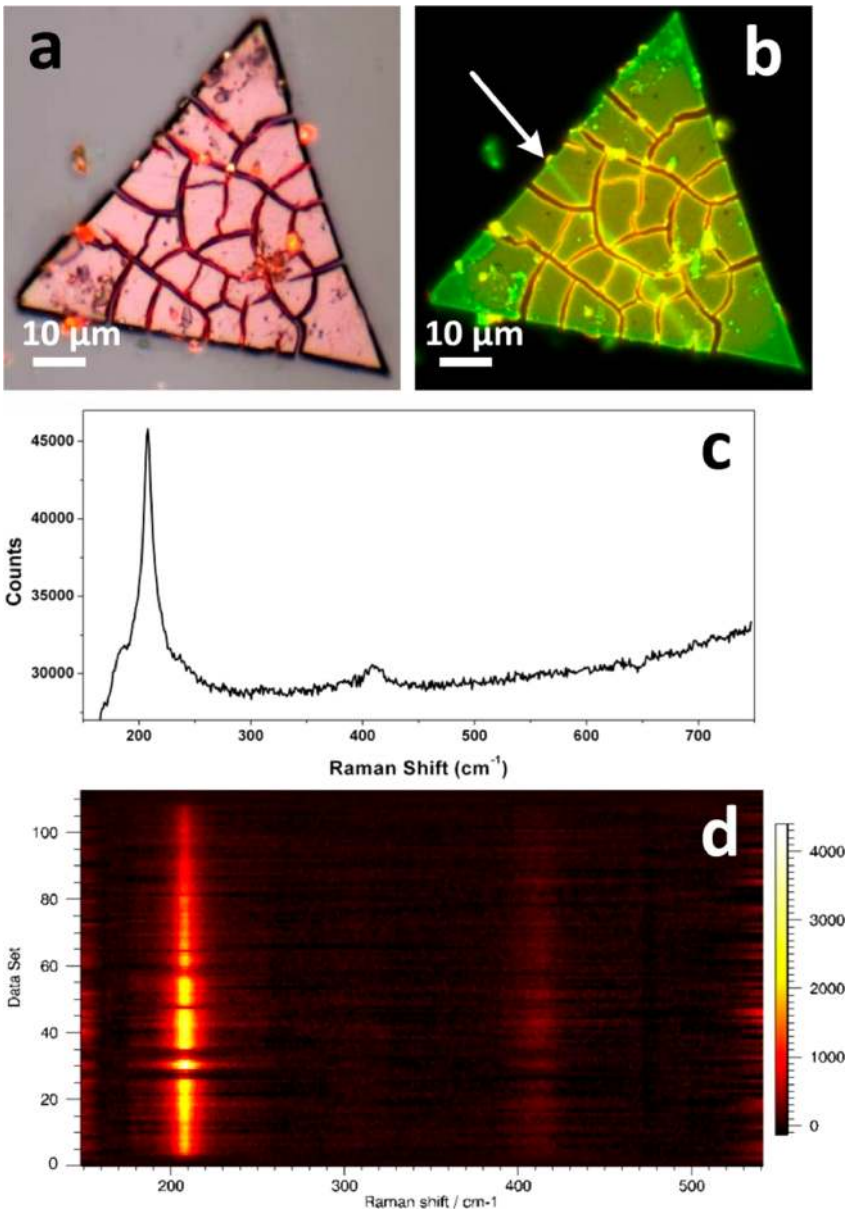

Figure 4. (a,b) Reflected light optical micrograph (a) and corresponding fluorescence image (b) of a supercrystal formed from 4.4 nm CdSe nanocrystals. (c) Representative Raman spectrum from the supercrystal, showing the CdSe LO (208 cm^{-1}), 2LO (420 cm^{-1}), and surface (188 cm^{-1}) phonon peaks. (d) Two-dimensional Raman scattering intensity map taken along the line indicated by the white arrow in (b). The color bar corresponds to the intensity of the Raman signal, in arbitrary units. Interruptions in the Raman map correspond to cracks in the SC. The fluorescence image in (b) was taken after the Raman map was acquired, and green emission can be seen along the path of the line.

driven by depletion interactions.[31] Indeed, previous studies of CdSe NC SCs assembled from polydisperse colloidal solutions showed size selection of NCs during SC assembly.[24] However, TEM images (Figures 1a and S1) show no evidence of polydispersity in the NC samples that we used. Moreover, when we deliberately mixed solutions of different-sized NCs and formed SCs from these solutions, we observed only single-color SCs (Figure S7). That is, mixtures of NCs that are "orange" and "green" because of their different diameters form separate orange and green SCs and do not form the two-color SCs that form from monodisperse NC solutions. We also note that there are only two distinct emission wavelengths for the two-color SCs: different points within the "orange" regions all emit at the same wavelength, and different points within the "green" regions all emit at the same wavelength (Figure S8). This is different from the continuous variation in emission wavelength that one would expect to arise from size segregation of a polydisperse sample.

A second potential explanation for the different emission colors is a difference in the packing of NCs in the different regions of the SCs, which would lead to different electronic coupling among the NCs. However, spatially resolved small-angle X-ray scattering measurements on individual SCs do not reveal significant changes in the packing of NCs between the orange and green regions (Figure 3).

Another possible explanation for the different emission colors is differences in strain within the orange and green regions. Indeed, it was previously reported that both

https://dx.doi.org/10.1021/acsnano.0c04864
ACS Nano XXXX, XXX, XXX−XXX

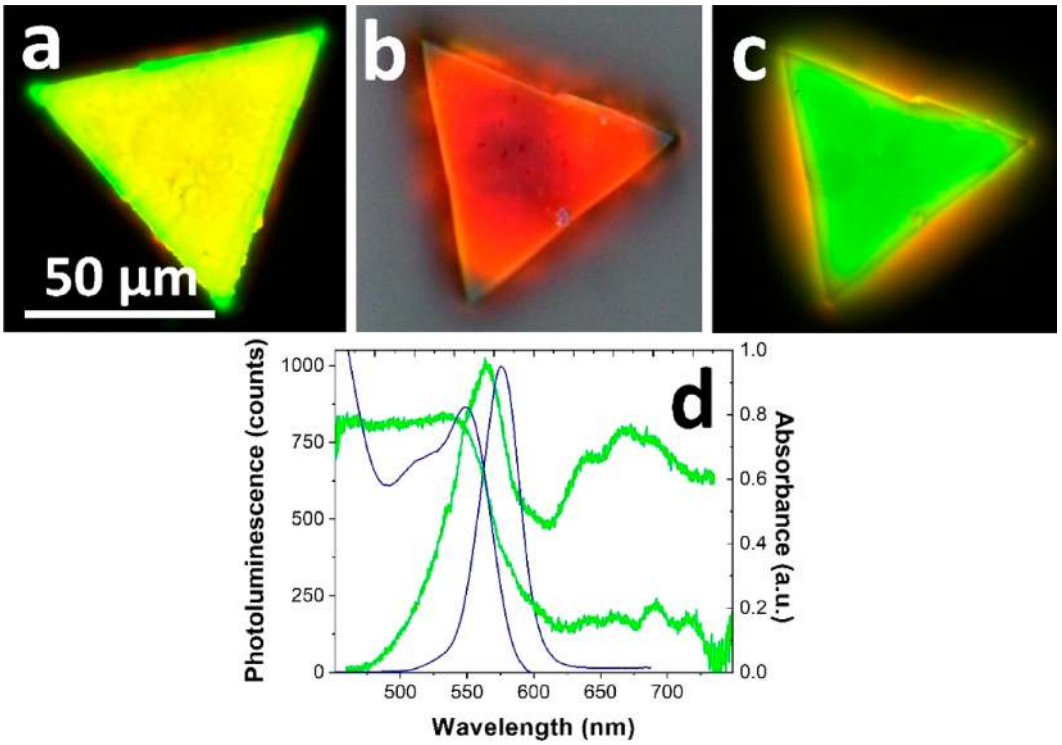

Figure 5. (a) Fluorescence image of a supercrystal formed from 4.4 nm CdSe nanocrystals before pyridine treatment. (b,c) Reflected light optical micrograph (b) and corresponding fluorescence image (c) of a supercrystal after pyridine treatment. (d) Absorption and photoluminescence spectra measured from a single supercrystal after pyridine treatment (shorter wavelength, green lines) and for nanocrystals in solution (longer wavelength, blue lines).

absorption and PL spectra can be blue-shifted by compressive strain of NCs,[32] and previous Raman microprobe studies have revealed large strains of ~2.5% for CdSe NCs in films.[33] Crack formation was proposed as a strain-relief mechanism for the films;[33] however, we observe two-color PL even from SCs with cracks (Figure 4a,b). Moreover, spatially resolved Raman spectroscopy shows no shift in the Raman peak position across the orange and green domains (Figure 4c,d), indicating the absence of strain within the CdSe NCs. Therefore, cracks are likely formed as a result of the evaporation of the solvent retained in the ligand shells of the self-assembled NCs upon their drying.[34,35]

On the other hand, the fluorescence image of the SC after the spatially resolved Raman measurement provides a clue about the origin of the green PL: a green line appears where the excitation laser was scanned across the sample (Figure 4b). This line is likely formed as a result of photo-oxidation of NCs in the SC.[36] Oxidation reduces the effective diameter of the NCs by replacing a surface semiconductor layer with oxides,[37] thereby increasing the confinement energy and increasing the effective band gap. This observation suggests that the NCs within the green regions of the SCs have oxidized compared to the NCs within the orange regions of the same SCs.

It is worth noting that a significant blue shift of 12 nm and considerable broadening, by 15 nm, compared to the initial NC colloidal solution was recently reported for CdSe SCs assembled by evaporation of CdSe NC solution.[38] Although the authors did not explain the observed blue shift, their results are in agreement with the progressive oxidation of individual CdSe NCs.

To verify whether oxidation is responsible for the observed blue shifts in the outer portions of the SCs, we treated our SCs with a 0.01 M solution of pyridine in toluene for 1 h. Exposure of CdSe SCs to pyridine solution is known to reduce the protection of the surfaces of CdSe NCs and thus make the surfaces more easily oxidized.[39] Indeed, the two-color SC emits nearly exclusively green light after pyridine treatment, and its PL and absorption spectra are both shifted to shorter wavelengths throughout the nanocrystal as compared to NCs in solution (Figure 5). This indicates that, once ligands are partially removed from the NCs in the central portion of the SCs, they undergo the same partial oxidation already undergone by the NCs in the outer portion of the SCs.

In other words, these results indicate that the green and orange regions of the SC are composed, respectively, of NCs that have and have not been partially oxidized. This, in turn, suggests that there are two subpopulations of NCs that are differently subject to oxidation. The most likely reason that one subpopulation would be more susceptible to oxidation than the other is that it has lower ligand coverage. The explanation that the green-emitting regions correspond to NCs with lower ligand coverage also explains why these NCs are located on the outer regions of the SCs: the lower ligand coverage provides higher solvation of the ligand shells and thus lower entropy gain through NC interactions when the colloidal solution is destabilized.[34,40] Indeed, it is well-known that differences in ligand coverage can affect the interactions among NCs;[34,41,42] as ligand−ligand interactions are one of the key factors determining the NC self-assembly process,[7,43−45] these differences in coverage will drive differences in the formation of supercrystals. Previously, it was shown that high ligand densities at the NC surface are associated with ligand and solvent ordering, resulting in a deep attractive minima near the NC contact.[46] In turn, at low surface coverage, the ligands are

https://dx.doi.org/10.1021/acsnano.0c04864
ACS Nano XXXX, XXX, XXX−XXX

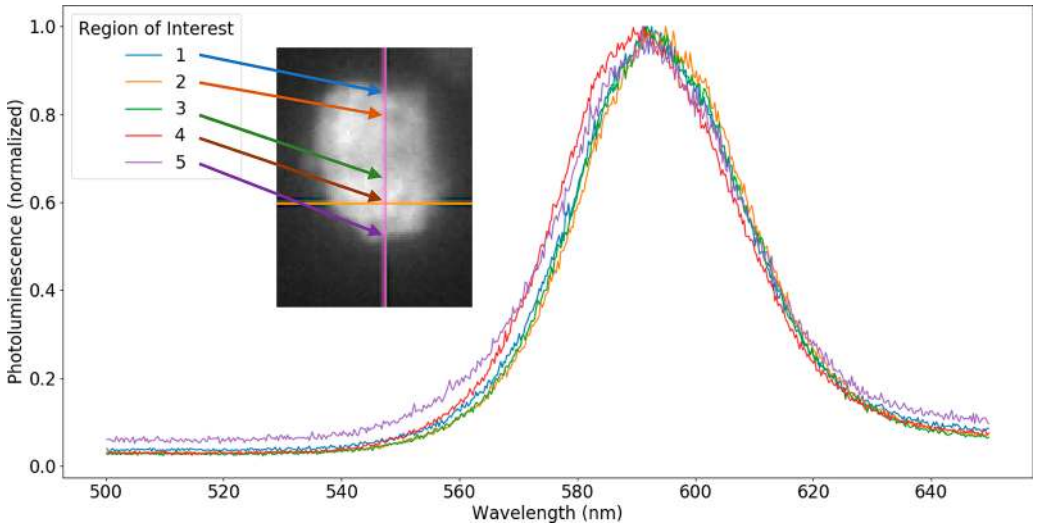

Figure 6. Spatially resolved photoluminescence spectra from a single supercrystal formed from 4.9 nm CdSe nanocrystals that were synthesized at 380 °C. Spectra were measured from five different points on the nanocrystal, as indicated in the inset, with a spatial resolution of approximately 200 nm.

disordered, and this was anticipated to give rise to repulsive surface forces in solution.[46]

In other words, the NCs with fewer ligands precipitate out of solution later than the ones with more ligands and are deposited at the edges of the SCs. During the slow deposition process, these nanocrystals are partially oxidized, shifting their absorption and luminescence to shorter wavelengths.

Alternatively, it is possible that the "green" NCs have some of their surface atoms displaced upon mixing of the NC solution with nonsolvent. Leaching of the atoms from NCs as a result of solvent/nonsolvent purification was previously reported,[47] and the stoichiometry of cadmium chalcogenides is known to be dynamic in nature and depend on various parameters, including solvents and nonsolvents used to purify NCs.[48] On the other hand, CdSe NCs synthesized using reaction conditions similar to those in this work and dissolved in chloroform did not show any change in size and stoichiometry upon extensive ligand removal using methanol.[49] Therefore, oxidation of less protected CdSe NCs is likely to be the main reason responsible for the green emission from these NCs.

As it is known that the synthesis method that we followed can lead to NCs with both ZB and W phases, we hypothesize that the differences in ligand coverage arise because of differences in the crystal phases of the CdSe NCs. Polytypism is known to be common in II–VI semiconducting NCs.[50] For CdSe, the energy difference between cubic ZB and hexagonal W crystalline phases is only 1.4 meV/atom,[51] which makes synthesis of pure crystalline phase NCs challenging.[52,53] The ratio of the ZB and W phase is sensitive to the experimental conditions, such as temperature, with CdSe NCs synthesized at lower temperature were reported to have ZB lattice structure, whereas high temperature favors the formation of particles with a W lattice structure.[54−56] Moreover, individual NCs can have stacking faults which locally induce a phase change, and hence, both phases can be present in the same NCs.[57,58]

Also playing important roles are the choice of surface ligands;[20,52,57,59−61] in fact, transitions between the ZB and W phases can be induced by introducing different ligands[52,59] or by changing the NC surface,[62] and the phase of CdSe NCs can depend even on the length of the ligands.[52] Conversely, NCs of the same size and composition but with different phases, or with different phases present on their surfaces, can have different ligand coverages of their surfaces.[63] For example, NMR studies on CdS NCs of similar sizes revealed that CdS NCs with ZB structure had lower ligand coverage by a factor of 4 as compared to NCs with W structure.[63] This different ligand coverage, in turn, can influence the solvation of the NC ligand shells[40] and thus the interactions among NCs.[34,41,42] As ligand–ligand interactions are one of the key factors determining the NC self-assembly process,[7,43−45] polytypism has the potential to significantly affect CdSe NC self-assembly.

We thus hypothesize that the oxidized and unoxidized NCs correspond to NCs terminated differently as a result of coexistence of NCs with two different phases such W and ZB (or pseudo-ZB,[56] a phase with a high density of stacking faults). We note that this hypothesis is supported by previous X-ray photoelectron spectroscopic studies, which indicated that the surface of ZB-CdSe is enriched with Cd^{2+} ions, which tend to lead to the formation of a CdO shell; this oxidation, in turn, results in a blue shift.[64] These studies are consistent with our results. We suggest that the oxidized and unoxidized NCs correspond to NCs terminated differently as a result of coexistence of NCs with two different phases such W and ZB (or pseudo-ZB,[56] a phase with a high density of stacking faults).

To test our hypothesis, we assembled SCs from CdSe NCs synthesized under conditions that provide a better control over the phase.[4] Specifically, we use a higher-temperature synthesis, which has been found to favor the formation of a single W phase of CdSe.[65,66] Although there is a discrepancy in the literature regarding the ZB–W transition temperature,[54] the general trend is that higher synthesis temperature favors the formation of the thermodynamically stable W phase of CdSe.[54−56] We therefore synthesized ~4.9 nm CdSe NCs at 370 or 380 °C using TOPO/TOP/ODPA ligands[4] and compared their X-ray diffraction (XRD) to that of the CdSe NCs synthesized at 310 °C using TOPO/TOP/HDA ligands. The XRD shows that the NCs synthesized at higher temperature contain a significantly lower fraction of the ZB phase (Figure S9).

https://dx.doi.org/10.1021/acsnano.0c04864
ACS Nano XXXX, XXX, XXX–XXX

The CdSe NCs synthesized at 380 °C and characterized by the lowest amount of ZB phase can thus serve as a control sample. We assembled these NCs into SCs, following the same procedure used for assembly of CdSe NCs synthesized at 310 °C.[19] No noticeable shift of the PL spectra was observed across individual SCs (Figure 6), supporting the hypothesis that the appearance of two-color domains in SCs assembled from CdSe synthesized at lower temperature is associated with the polymorphism of CdSe NCs.

CONCLUSIONS

Assembly of monodisperse CdSe nanocrystals into three-dimensional supercrystals by the controlled oversaturation method leads to SCs with distinct regions whose photoluminescence and absorption are shifted to the red and to the blue, respectively, compared to the NCs in solution. Our spectroscopic evidence indicates that the blue-shifted domains are composed of partially oxidized NCs. The monodisperse sample of CdSe NCs thus contains two subpopulations, one of which (1) precipitates into the SCs later than the other subpopulation and (2) is susceptible to oxidation, unlike the other subpopulation. These observations are both consistent with one subpopulation having a lower ligand coverage than the other. Considering the bimodal nature of optical absorption and emission observed in SCs assembled from CdSe NCs synthesized at 310 °C, we hypothesize that this difference in ligand coverage is due to coexistence of two types of CdSe NCs, whose surfaces have W and ZB lattice structures.

Whereas our XRD measurements clearly indicate a higher ZB fraction in CdSe NCs synthesized at lower temperature, they suggest that there is still some ZB content even for the NCs synthesized at 380 °C. However, taking into account the well-documented tendency of CdSe NCs to have stacking faults because of the small energy difference between ZB and W phases, it is likely that some individual NCs contain both phases.[57,58] For NCs synthesized at 310 °C, the two subpopulations may correspond to NCs with different locally induced phases at their surfaces; these different surface phases would then result in different ligand coverages. The segregation of NCs in SCs according to their ligand coverage and the corresponding blue shift of emission from the less-protected NCs provide a straightforward method for visualizing and possibly quantifying otherwise hidden differences among monodisperse NCs.

METHODS

Materials. Toluene, isopropyl alcohol (*i*-PrOH), diphenyl ether, ethanol, *n*-hexane, trioctylphosphine oxide (TOPO), hexadecylamine (HDA), octadecylphosphonic acid (ODPA), bis(trimethylsilyl)sulfide ($(TMS)_2S$), and sulfur were all purchased from Sigma-Aldrich and were at least of ACS purity. Trioctylphosphine (TOP) and 1,2-hexadecandiol were obtained from Fluka. 1,2-Dichlorobenzene was purchased from Acros Chemicals. Four inch Si wafers used for growing the SCs were obtained from Silicon Quest International, Inc. (Santa Clara, CA). The Si wafers were diced into 4 mm wide strips with a wafer dicing saw. Glass test tubes (0.8 cm i.d. by 10 cm long) used for SC growth were obtained from Fisher Scientific.

Nanocrystal Synthesis. The 4.6 and 4.4 nm CdSe NCs stabilized with TOPO/TOP/HDA and TOPO/TOP/ODPA were synthesized according to the protocol described in ref 19. The 4.9 nm CdSe NCs were synthesized at 380 °C.[4] Samples for TEM characterization were prepared by placing 1−2 μL of a diluted (0.1 mg/mL) solution in toluene on a carbon-coated copper grid (Ted-Pella). The excess solvent was removed after 10 s with filter paper.

Preparation of Nanocrystal Supercrystals. The SCs were prepared by the method of slow destabilization of NCs with a nonsolvent.[19] In a typical preparation, a single strip of Si or ITO-coated glass was placed vertically in a vertically positioned glass test tube, and 0.5 mL of a moderately concentrated NC solution (~1×10^{12} NCs/mL) in toluene was added to the bottom with a micropipettor. Subsequently, 0.8 mL of *i*-PrOH was gently added on top of the NC solution, avoiding intermixing of the two solutions. The tubes were then sealed with Parafilm and allowed to sit undisturbed for a week. After a complete diffusional intermixing of the solvents, the solutions were carefully withdrawn with Pasteur pipettes and discarded. The substrates were removed, air-dried, and stored for subsequent characterization. NC films were obtained by evaporation of the same toluene solutions on the surface of ITO-coated glass.

Characterization Methods. Transmission electron microscope images were obtained using a FEI Tecnai F30 field-emission analytical TEM operating at an acceleration voltage of 300 kV. High-resolution scanning electron microscopy images were obtained with an FIB FEI Nova 600 NanoLab SEM operated at 18 keV accelerating voltage.

Optical images were obtained with a Zeiss Axio Imager microscope. Fluorescence images were collected with an excitation light source with wavelengths between 320 and 460 nm and with emission collected for wavelengths above 465 nm.

Confocal microscope images and cross sections were collected using a Zeiss LSM 510 Meta confocal microscope. The particles were excited using 488 or 561 nm laser light, and emission was monitored in the ranges of 500−550 or 575−625 nm.

Raman spectra were measured on a Renishaw inVia Raman microscope with excitation wavelength of 514 or 613 nm, power of 5 mW, and a spot size of ~ 1 μm. All spectra were measured using a 100× microscope objective to focus the laser excitation onto the samples and to collect the scattered light.

Spatially resolved spectra were measured on a home-built inverted microscope. For spatially resolved PL spectra, the sample was illuminated through the microscope objective with a short wavelength (<500 nm) laser focused to a diffraction-limited spot (approximately 200 nm spot size), and emitted light was collected through the same objective and sent to a grating spectrometer with a CCD camera detector. Time-resolved PL was measured by using the time-correlated single-photon detection technique in place of the spectrometer. For spatially resolved absorption spectra, the sample was illuminated in transmission mode by a bright-field condenser, and specific spots on the sample were selected for measurement by using the entrance slit of the spectrometer and by selecting pixels on the array detector. The measured transmitted spectra were normalized by spectra measured away from the SCs to obtain absorption spectra. The resolution of the absorption measurements matches the diffraction-limited resolution of the PL measurements.

The small-angle X-ray scattering data were acquired at the 12-ID-B beamline of the Advanced Photon Source at Argonne National Laboratory. The X-ray beam had an energy of 14 keV, wavelength λ = 0.8856 Å, and size of 10 × 10 μm. Each spot was exposed to the beam for 1 s. The sample to detector distance was approximately 2 m. Absolute intensity was calculated using water as a standard.

Powder X-ray diffraction data were acquired using a Bruker D2 Phaser on CdSe NC films deposited by evaporation of toluene solutions.

ASSOCIATED CONTENT

Supporting Information

The Supporting Information is available free of charge at https://pubs.acs.org/doi/10.1021/acsnano.0c04864.

Transmission electron microscopy image of 4.4 nm CdSe nanocrystals; size histograms obtained for 4.4 and 4.6 nm CdSe NCs; scanning electron microscopy images of supercrystals; laser scanning confocal microscopy image of three-dimensional supercrystals; thermogravimetric analysis of films and supercrystals formed from

https://dx.doi.org/10.1021/acsnano.0c04864
ACS Nano XXXX, XXX, XXX−XXX

the same nanocrystals; fluorescence images of three-dimensional supercrystals formed from mixtures of CdSe nanocrystals with two different sizes; spatially resolved photoluminescence spectra from orange-emitting and green-emitting regions of three-dimensional supercrystals; powder X-ray diffraction data for CdSe nanocrystals synthesized at different temperatures (PDF)

AUTHOR INFORMATION

Corresponding Authors

Elena V. Shevchenko − *Center for Nanoscale Materials, Argonne National Laboratory, Argonne, Illinois 60439, United States;* orcid.org/0000-0002-5565-2060; Email: eshevchenko@anl.gov

Matthew Pelton − *Center for Nanoscale Materials, Argonne National Laboratory, Argonne, Illinois 60439, United States; Department of Physics, UMBC (University of Maryland, Baltimore County), Baltimore, Maryland 20912, United States;* orcid.org/0000-0002-6370-8765; Email: mpelton@umbc.edu

Authors

Paul Podsiadlo − *Center for Nanoscale Materials, Argonne National Laboratory, Argonne, Illinois 60439, United States; ExxonMobil Research and Engineering Company, Fuels, Process & Optimization Technology Process Engineering Division, Parkway Spring, Texas 77389, United States*

Xiaohua Wu − *Center for Nanoscale Materials, Argonne National Laboratory, Argonne, Illinois 60439, United States; Mindray, Shenzhen 518057, China*

Byeongdu Lee − *Advanced Photon Source, Argonne National Laboratory, Argonne, Illinois 60439, United States;* orcid.org/0000-0003-2514-8805

Tijana Rajh − *Center for Nanoscale Materials, Argonne National Laboratory, Argonne, Illinois 60439, United States*

Rachel Morin − *Department of Physics, UMBC (University of Maryland, Baltimore County), Baltimore, Maryland 20912, United States*

Complete contact information is available at: https://pubs.acs.org/10.1021/acsnano.0c04864

Notes

The authors declare no competing financial interest.

ACKNOWLEDGMENTS

We thank Prof. Emily Weiss (Northwestern University) for helpful conversations. Work at the Center for Nanoscale Materials and the Advanced Photon Source was supported by the U.S. Department of Energy, Office of Science, Office of Basic Energy Sciences, under Contract No. DE-AC0206CH-11357.

REFERENCES

(1) Murray, C. B.; Norris, D. J.; Bawendi, M. G. Synthesis and Characterization of Nearly Monodisperse CdE (E = Sulfur, Selenium, Tellurium) Semiconductor Nanocrystallites. *J. Am. Chem. Soc.* **1993**, *115*, 8706−8715.

(2) Murray, C. B.; Kagan, C. R.; Bawendi, M. G. Self-Organization of CdSe Nanocrystallites into Three-Dimensional Quantum Dot Superlattices. *Science* **1995**, *270*, 1335−1338.

(3) Talapin, D. V.; Nelson, J. H.; Shevchenko, E. V.; Aloni, S.; Sadtler, B.; Alivisatos, A. P. Seeded Growth of Highly Luminescent CdSe/CdS Nanoheterostructures with Rod and Tetrapod Morphologies. *Nano Lett.* **2007**, *7*, 2951−2959.

(4) Carbone, L.; Nobile, C.; De Giorgi, M.; Sala, F. D.; Morello, G.; Pompa, P.; Hytch, M.; Snoeck, E.; Fiore, A.; Franchini, I. R.; Nadasan, M.; Silvestre, A. F.; Chiodo, L.; Kudera, S.; Cingolani, R.; Krahne, R.; Manna, L. Synthesis and Micrometer-Scale Assembly of Colloidal CdSe/CdS Nanorods Prepared by a Seeded Growth Approach. *Nano Lett.* **2007**, *7*, 2942−2950.

(5) Abécassis, B.; Tessier, M. D.; Davidson, P.; Dubertret, B. Self-Assembly of CdSe Nanoplatelets into Giant Micrometer-Scale Needles Emitting Polarized Light. *Nano Lett.* **2014**, *14*, 710−715.

(6) Antanovich, A.; Prudnikau, A.; Matsukovich, A.; Achtstein, A.; Artemyev, M. Self-Assembly of CdSe Nanoplatelets into Stacks of Controlled Size Induced by Ligand Exchange. *J. Phys. Chem. C* **2016**, *120*, 5764−5775.

(7) Jana, S.; de Frutos, M.; Davidson, P.; Abécassis, B. Ligand-Induced Twisting of Nanoplatelets and Their Self-Assembly into Chiral Ribbons. *Sci. Adv.* **2017**, *3*, No. e1701483.

(8) Kim, D.; Bae, W. K.; Kim, S.-H.; Lee, D. C. Depletion-Mediated Interfacial Assembly of Semiconductor Nanorods. *Nano Lett.* **2019**, *19*, 963−970.

(9) Boles, M. A.; Engel, M.; Talapin, D. V. Self-Assembly of Colloidal Nanocrystals: From Intricate Structures to Functional Materials. *Chem. Rev.* **2016**, *116*, 11220−11289.

(10) Murray, C. B.; Kagan, C. R.; Bawendi, M. G. Synthesis and Characterization of Monodisperse Nanocrystals and Close-Packed Nanocrystal Assemblies. *Annu. Rev. Mater. Sci.* **2000**, *30*, 545−610.

(11) Shevchenko, E. V.; Talapin, D. V.; Kotov, N. A.; O'Brien, S.; Murray, C. B. Structural Diversity in Binary Nanoparticle Superlattices. *Nature* **2006**, *439*, 55.

(12) Dong, A.; Chen, J.; Vora, P. M.; Kikkawa, J. M.; Murray, C. B. Binary Nanocrystal Superlattice Mmembranes Self-Assembled at the Liquid−Air Interface. *Nature* **2010**, *466*, 474.

(13) Baker, J. L.; Widmer-Cooper, A.; Toney, M. F.; Geissler, P. L.; Alivisatos, A. P. Device-Scale Perpendicular Alignment of Colloidal Nanorods. *Nano Lett.* **2010**, *10*, 195−201.

(14) Rainò, G.; Becker, M. A.; Bodnarchuk, M. I.; Mahrt, R. F.; Kovalenko, M. V.; Stöferle, T. Superfluorescence from Lead Halide Perovskite Quantum Dot Superlattices. *Nature* **2018**, *563*, 671−675.

(15) Shevchenko, E. V.; Talapin, D. V.; Rogach, A. L.; Kornowski, A.; Haase, M.; Weller, H. Colloidal Synthesis and Self-Assembly of $CoPt_3$ Nanocrystals. *J. Am. Chem. Soc.* **2002**, *124*, 11480−11485.

(16) Talapin, D. V.; Shevchenko, E. V.; Kornowski, A.; Gaponik, N.; Haase, M.; Rogach, A. L.; Weller, H. A New Approach to Crystallization of CdSe Nanoparticles into Ordered Three-Dimensional Superlattices. *Adv. Mater.* **2001**, *13*, 1868−1871.

(17) Podsiadlo, P.; Krylova, G.; Lee, B.; Critchley, K.; Gosztola, D. J.; Talapin, D. V.; Ashby, P. D.; Shevchenko, E. V. The Role of Order, Nanocrystal Size, and Capping Ligands in the Collective Mechanical Response of Three-Dimensional Nanocrystal Solids. *J. Am. Chem. Soc.* **2010**, *132*, 8953−8960.

(18) Chen, J.; Lim, B. K.; Lee, E. P.; Xia, Y. Shape-Controlled Synthesis of Platinum Nanocrystals for Catalytic and Electrocatalytic Applications. *Nano Today* **2009**, *4*, 81−95.

(19) Talapin, D. V.; Rogach, A. L.; Kornowski, A.; Haase, M.; Weller, H. Highly Luminescent Monodisperse CdSe and CdSe/ZnS Nanocrystals Synthesized in a Hexadecylamine−Trioctylphosphine Oxide−Trioctylphospine Mixture. *Nano Lett.* **2001**, *1*, 207−211.

(20) Rupich, S. M.; Shevchenko, E. V.; Bodnarchuk, M. I.; Lee, B.; Talapin, D. V. Size-Dependent Multiple Twinning in Nanocrystal Superlattices. *J. Am. Chem. Soc.* **2010**, *132*, 289−296.

(21) Talapin, D. V.; Shevchenko, E. V.; Murray, C. B.; Titov, A. V.; Kral, P. Dipole-Dipole Interactions in Nanoparticle Superlattices. *Nano Lett.* **2007**, *7*, 1213−1219.

(22) Shevchenko, E. V.; Talapin, D. V.; Murray, C. B.; O'Brien, S. Structural Characterization of Self-Assembled Multifunctional Binary Nanoparticle Superlattices. *J. Am. Chem. Soc.* **2006**, *128*, 3620−3637.

(23) Paik, T.; Diroll, B. T.; Kagan, C. R.; Murray, C. B. Binary and Ternary Superlattices Self-Assembled from Colloidal Nanodisks and Nanorods. *J. Am. Chem. Soc.* **2015**, *137*, 6662−6669.
(24) Zaitseva, N.; Dai, Z. R.; Leon, F. R.; Krol, D. Optical Properties of CdSe Superlattices. *J. Am. Chem. Soc.* **2005**, *127*, 10221−10226.
(25) Kholmicheva, N.; Moroz, P.; Eckard, H.; Jensen, G.; Zamkov, M. Energy Transfer in Quantum Dot Solids. *ACS Energy Lett.* **2017**, *2*, 154−160.
(26) Lingley, Z.; Lu, S.; Madhukar, A. The Dynamics of Energy and Charge Transfer in Lead Sulfide Quantum Dot Solids. *J. Appl. Phys.* **2014**, *115*, No. 084302.
(27) Bawendi, M. G.; Carroll, P. J.; Wilson, W. L.; Brus, L. E. Luminescence Properties of CdSe Quantum Crystallites: Resonance Between Interior and Surface Localized States. *J. Chem. Phys.* **1992**, *96*, 946−954.
(28) Kagan, C. R.; Murray, C. B.; Nirmal, M.; Bawendi, M. G. Electronic Energy Transfer in CdSe Quantum Dot Solids. *Phys. Rev. Lett.* **1996**, *76*, 1517−1520.
(29) Das, T. K.; Ilaiyaraja, P.; Sudakar, C. Coexistence of Strongly and Weakly Confined Energy Levels in (Cd,Zn)Se Quantum Dots: Tailoring the Near-Band-Edge and Defect-Levels for White Light Emission. *J. Appl. Phys.* **2017**, *121*, 183102.
(30) Rabani, E.; Hetényi, B.; Berne, B. J.; Brus, L. E. Electronic Properties of CdSe Nanocrystals in the Absence and Presence of a Dielectric Medium. *J. Chem. Phys.* **1999**, *110*, 5355−5369.
(31) Yodh, A. G.; Lin, K.; Crocker, J. C.; Dinsmore, A. D.; Verma, R.; Kaplan, P. D. Entropically Driven Self-Assembly and Interaction in Suspension. *Philos. Trans. R. Soc., A* **2001**, *359*, 921−937.
(32) Cho, J.; Kim, Y. J.; Kim, T.-J.; Park, B. Zero-Strain Intercalation Cathode for Rechargeable Li-Ion Cell. *Angew. Chem., Int. Ed.* **2001**, *40*, 3367−3369.
(33) Banerjee, S.; Jia, S.; Kim, D. I.; Robinson, R. D.; Kysar, J. W.; Bevk, J.; Herman, I. P. Raman Microprobe Analysis of Elastic Strain and Fracture in Electrophoretically Deposited CdSe Nanocrystal Films. *Nano Lett.* **2006**, *6*, 175−180.
(34) Lee, B.; Littrell, K.; Sha, Y.; Shevchenko, E. V. Revealing the Effects of the Non-Solvent on the Ligand Shell of Nanoparticles and Their Crystallization. *J. Am. Chem. Soc.* **2019**, *141*, 16651−16662.
(35) Schneider, M.; Maurath, J.; Fischer, S. B.; Weiß, M.; Willenbacher, N.; Koos, E. Suppressing Crack Formation in Particulate Systems by Utilizing Capillary Forces. *ACS Appl. Mater. Interfaces* **2017**, *9*, 11095−11105.
(36) Manner, V. W.; Koposov, A. Y.; Szymanski, P.; Klimov, V. I.; Sykora, M. Role of Solvent−Oxygen Ion Pairs in Photooxidation of CdSe Nanocrystal Quantum Dots. *ACS Nano* **2012**, *6*, 2371−2377.
(37) Hines, D. A.; Becker, M. A.; Kamat, P. V. Photoinduced Surface Oxidation and Its Effect on the Exciton Dynamics of CdSe Quantum Dots. *J. Phys. Chem. C* **2012**, *116*, 13452−13457.
(38) Ushakova, E. V.; Cherevkov, S. A.; Volgina, D.-O. A.; Zakharov, V. V.; Komissarenko, F. E.; Shcherbakov, A. A.; Hogan, B. T.; Baldycheva, A.; Fedorov, A. V.; Nabiev, I. R.; Baranov, A. V. From Colloidal CdSe Quantum Dots to Microscale Optically Anisotropic Supercrystals Through Bottom-Up Self-Assembly. *J. Mater. Chem. C* **2018**, *6*, 12904−12911.
(39) Luo, X.; Liu, P.; Truong, N. T. N.; Farva, U.; Park, C. Photoluminescence Blue-Shift of CdSe Nanoparticles Caused by Exchange of Surface Capping Layer. *J. Phys. Chem. C* **2011**, *115*, 20817−20823.
(40) Kaushik, A. P.; Clancy, P. Solvent-Driven Symmetry of Sself-Assembled Nanocrystal Superlattices—A Computational Study. *J. Comput. Chem.* **2013**, *34*, 523−532.
(41) Waltmann, C.; Horst, N.; Travesset, A. Capping Ligand Vortices as "Atomic Orbitals" in Nanocrystal Self-Assembly. *ACS Nano* **2017**, *11*, 11273−11282.
(42) Si, K. J.; Chen, Y.; Shi, Q.; Cheng, W. Nanoparticle Superlattices: The Roles of Soft Ligands. *Adv. Sci.* **2018**, *5*, 1700179.
(43) Zeng, X.; Liu, F.; Fowler, A. G.; Ungar, G.; Cseh, L.; Mehl, G. H.; Macdonald, J. E. 3D Ordered Gold Strings by Coating Nanoparticles with Mesogens. *Adv. Mater.* **2009**, *21*, 1746−1750.
(44) Guo, S.; Li, D.; Zhu, H.; Zhang, S.; Markovic, N. M.; Stamenkovic, V. R.; Sun, S. FePt and CoPt Nanowires as Efficient Catalysts for the Oxygen Reduction Reaction. *Angew. Chem., Int. Ed.* **2013**, *52*, 3465−3468.
(45) Macfarlane, R. J.; Lee, B.; Jones, M. R.; Harris, N.; Schatz, G. C.; Mirkin, C. A. Nanoparticle Superlattice Engineering with DNA. *Science* **2011**, *334*, 204−208.
(46) Widmer-Cooper, A.; Geissler, P. L. Ligand-Mediated Interactions between Nanoscale Surfaces Depend Sensitively and Nonlinearly on Temperature, Facet Dimensions, and Ligand Coverage. *ACS Nano* **2016**, *10*, 1877−1887.
(47) Mizrahi, M. D.; Krylova, G.; Giovanetti, L. J.; Ramallo-López, J. M.; Liu, Y.; Shevchenko, E. V.; Requejo, F. G. Unexpected Compositional and Structural Modification of $CoPt_3$ Nanoparticles by Extensive Surface Purification. *Nanoscale* **2018**, *10*, 6382−6392.
(48) Anderson, N. C.; Hendricks, M. P.; Choi, J. J.; Owen, J. S. Ligand Exchange and the Stoichiometry of Metal Chalcogenide Nanocrystals: Spectroscopic Observation of Facile Metal-Carboxylate Displacement and Binding. *J. Am. Chem. Soc.* **2013**, *135*, 18536−18548.
(49) Morris-Cohen, A. J.; Donakowski, M. D.; Knowles, K. E.; Weiss, E. A. The Effect of a Common Purification Procedure on the Chemical Composition of the Surfaces of CdSe Quantum Dots Synthesized with Trioctylphosphine Oxide. *J. Phys. Chem. C* **2010**, *114*, 897−906.
(50) Manna, L.; Milliron, D. J.; Meisel, A.; Scher, E. C.; Alivisatos, A. P. Controlled Growth of Tetrapod-Branched Inorganic Nanocrystals. *Nat. Mater.* **2003**, *2*, 382−385.
(51) Yeh, C.-Y.; Lu, Z. W.; Froyen, S.; Zunger, A. Zinc-Blende–Wurtzite Polytypism in Semiconductors. *Phys. Rev. B: Condens. Matter Mater. Phys.* **1992**, *46*, 10086−10097.
(52) Huang, J.; Kovalenko, M. V.; Talapin, D. V. Alkyl Chains of Surface Ligands Affect Polytypism of CdSe Nanocrystals and Play an Important Role in the Synthesis of Anisotropic Nanoheterostructures. *J. Am. Chem. Soc.* **2010**, *132*, 15866−15868.
(53) Yu, W. W.; Peng, X. Formation of High-Quality CdS and Other II−VI Semiconductor Nanocrystals in Noncoordinating Solvents: Tunable Reactivity of Monomers. *Angew. Chem., Int. Ed.* **2002**, *41*, 2368−2371.
(54) Fedorov, V.; Ganshin, V.; Korkishko, Y. Determination of the Point of the Zincblende-To-Wurtzite Structural Phase Transition in Cadmium Selenide Crystals. *Phys. Status Solidi A* **1991**, *126*, K5−K7.
(55) Nan, W.; Niu, Y.; Qin, H.; Cui, F.; Yang, Y.; Lai, R.; Lin, W.; Peng, X. Crystal Structure Control of Zinc-Blende CdSe/CdS Core/Shell Nanocrystals: Synthesis and Structure-Dependent Optical Properties. *J. Am. Chem. Soc.* **2012**, *134*, 19685−19693.
(56) Washington, A. L.; Foley, M. E.; Cheong, S.; Quffa, L.; Breshike, C. J.; Watt, J.; Tilley, R. D.; Strouse, G. F. Ostwald's Rule of Stages and Its Role in CdSe Quantum Dot Crystallization. *J. Am. Chem. Soc.* **2012**, *134*, 17046−17052.
(57) Mahler, B.; Lequeux, N.; Dubertret, B. Ligand-Controlled Polytypism of Thick-Shell CdSe/CdS Nanocrystals. *J. Am. Chem. Soc.* **2010**, *132*, 953−959.
(58) Wang, X.; Chen, S.; Thota, S.; Wang, Y.; Tan, H.; Tang, M.; Quan, Z.; Zhao, J. Anisotropic Arm Growth in Unconventional Semiconductor CdSe/CdS Nanotetrapod Synthesis Using Core/Shell CdSe/CdS as Seeds. *J. Phys. Chem. C* **2019**, *123*, 19238−19245.
(59) Chai, Y.; Lu, J.; Li, L.; Li, D.; Li, M.; Liang, J. TEOA-Induced *in Situ* Formation of Wurtzite and Znc-Blende CdS Heterostructures as a Highly Active and Long-Lasting Photocatalyst for Converting CO_2 into Solar Fuel. *Catal. Sci. Technol.* **2018**, *8*, 2697−2706.
(60) Yang, Y. A.; Wu, H.; Williams, K. R.; Cao, Y. C. Synthesis of CdSe and CdTe Nanocrystals without Precursor Injection. *Angew. Chem., Int. Ed.* **2005**, *44*, 6712−6715.
(61) Wu, F.; Zhang, Z.; Zhu, Z.; Li, M.; Lu, W.; Chen, M.; Xu, E.; Wang, L.; Jiang, Y. Fine-Tuning the Crystal Structure of CdSe Quantum Dots by Varying the Dynamic Characteristics of Primary Alkylamine Ligands. *CrystEngComm* **2018**, *20*, 4492−4498.

https://dx.doi.org/10.1021/acsnano.0c04864
ACS Nano XXXX, XXX, XXX−XXX

(62) Soni, U.; Arora, V.; Sapra, S. Wurtzite or Zinc Blende? Surface Decides the Crystal Structure of Nanocrystals. *CrystEngComm* **2013**, *15*, 5458−5463.
(63) Davis, J. L.; Chalifoux, A. M.; Brock, S. L. Role of Crystal Structure and Chalcogenide Redox Properties on the Oxidative Assembly of Cadmium Chalcogenide Nanocrystals. *Langmuir* **2017**, *33*, 9434−9443.
(64) Subila, K. B.; Kishore Kumar, G.; Shivaprasad, S. M.; George Thomas, K. Luminescence Properties of CdSe Quantum Dots: Role of Crystal Structure and Surface Composition. *J. Phys. Chem. Lett.* **2013**, *4*, 2774−2779.
(65) Ansar, S. M.; Kitchens, C. L. Impact of Gold Nanoparticle Stabilizing Ligands on the Colloidal Catalytic Reduction of 4-Nitrophenol. *ACS Catal.* **2016**, *6*, 5553−5560.
(66) Christodoulou, S.; Vaccaro, G.; Pinchetti, V.; De Donato, F.; Grim, J. Q.; Casu, A.; Genovese, A.; Vicidomini, G.; Diaspro, A.; Brovelli, S.; Manna, L.; Moreels, I. Synthesis of Highly Luminescent Wurtzite CdSe/CdS Giant-Shell Nanocrystals Using a Fast Continuous Injection rRoute. *J. Mater. Chem. C* **2014**, *2*, 3439−3447.

https://dx.doi.org/10.1021/acsnano.0c04864
ACS Nano XXXX, XXX, XXX−XXX